



Modeling the seismic response of cold-formed steel framed buildings: model development for the CFS-NEES building

J. Leng¹, B. W. Schafer², S. G. Buonopane³

Abstract

The objective of this paper is to investigate the response of a cold-formed steel framed building subjected to earthquake excitation primarily through nonlinear time history analysis employing the incremental dynamic analysis (IDA) framework. The two-story archetype building from the Cold-Formed Steel – Network for Earthquake Engineering Simulation (CFS-NEES) project is analyzed using OpenSees. In the current ‘state-of-the-art’ model, fully nonlinear hysteretic pinching models for the shear walls are parameterized directly based on shear wall test data conducted as an earlier phase of the CFS-NEES project. Nonlinear behavior of the shear wall hold downs in tension and compression, shear anchors, and rigid diaphragm are also captured in the model. The normalized far field ground motion suite from FEMA P695 is employed as the input excitation. A series of analyses using scaled ground motions are completed up through large enough drift levels to insure collapse in the building models. The IDA procedure provides information about the performance of the building under general earthquake loading so that drift and other limits for collapse prevention (i.e. loss of stability for the building) can be explored. Comparison of the predicted inelastic base shear vs. elastic base shear provides a direct understanding of the relationship between IDA analysis and seismic response modification factors (e.g., R or more specifically R_d) as utilized in design practice and within the FEMA P695 procedure. Further refinement of the building model is underway; particularly, with respect to modeling the gravity framing, diaphragm, and non-structural elements. The fully developed model will be calibrated with test data from full scale shaking table tests of this building to be conducted in the summer of 2013. Modeling and analysis guidelines based on the sensitivity of the results to model fidelity will be developed as a resource to promote simulation in seismic design of cold-formed steel buildings.

1. Introduction

Light weight cold-formed steel (CFS) framing is an efficient and economical option for low and mid-rise buildings. However, forming moment connections in such thin-walled members is challenging, and the members themselves are subject to a variety of unique stability modes. By forming an assembly with closely spaced members covered by sheathing, the system can

¹ Graduate Research Assistant, Dept. of Civil Engineering, Johns Hopkins University, <jleng1@jhu.edu>

² Professor and Chair, Dept. of Civil Engineering, Johns Hopkins University, <schafer@jhu.edu>

³ Associate Professor, Dept. of Civil & Env. Engineering, Bucknell University, <sbuonopa@bucknell.edu>

efficiently resist lateral and gravity loads. Significant work remains for understanding the full building system behavior, especially under highly detrimental and unpredictable seismic excitations. The work presented herein is part of a National Science Foundation funded Cold-Formed Steel – Network for Earthquake Engineering Simulation (CFS-NEES) project that incorporates both full scale shaking table tests and detailed modeling of CFS framed buildings in an effort to address multi-story cold-formed steel lateral force resisting systems for modern performance-based seismic design. The research presented here is an advance from the authors' previous work (Leng et al., 2012) and provides a more refined 3D building model and initial results from incremental dynamic analysis (IDA) studies.

IDA, as proposed by Vamvatsikos and Cornell (2002), may be conceptualized as a dynamic extension of pushover analysis. By recording the structure's response under linearly scaled earthquake excitations the overall building response can be summarized. Typical structural response measures include story drifts and the spectral acceleration of the first natural period of the structure (S_a) is typically used for a simple scalar characterization of the earthquake intensity. Multiple ground motions are employed to account for record to record difference in the ground motion signals (Vamvatsikos and Cornell, 2004). Output from an IDA enables analysts to propose criterion for collapse prevention based on deformation measures and use statistics of the various excitations to evaluate the overall performance of a lateral force resisting system or building type. A detailed procedure is provided in the FEMA P695 report (Applied Technology Council, 2009). IDA and the nonlinear time history analysis that it requires is an enabling tool towards performance-based seismic design as it provides a probabilistic assessment of building damage (performance) as a function of input excitation.

In this paper, our 'state-of-the-art' simulation of the CFS-NEES building using OpenSees (McKenna et al., 2011) is summarized. Apart from the shear wall itself, additional influences including nonlinear modeling of the hold downs, leaning columns, and P- Δ effects are taken into account. Free vibration, pushover and IDA analyses are carried out using our 3D model. Tentative drift limits for collapse prevention are explored and the ratio between linear and nonlinear base shear is calculated to shed further light on seismic response modification factors for use in equivalent lateral force methods. Several factors that must be resolved in future modeling efforts are also introduced and discussed.

2. Features of CFS-NEES building models

As introduced in previous work (Leng et al. 2012), a professionally designed archetype building consisting of a two-story cold-formed steel frame, together with type I OSB sheathed shear walls and diaphragms as the major lateral force resisting system, is the focus of the CFS-NEES project (see Fig. 1). The building is assumed to be sited in Orange County, California. Details including design calculation and drawings are available in the combined narrative (Madsen et al. 2011). Gravity and lateral loads were determined per IBC (2009) which specifies ASCE 7-05. Cold-formed steel members were sized per American Iron and Steel Institute (AISI) Specifications (AISI-S100, -S210, -S211). The lateral force resisting system was also designed using an AISI specification (AISI-S213).

The footprint of the building is 23'0" x 49'9" [7.01 m x 15.16 m] and the height is 19'3" [5.88 m]. The gravity walls utilize an all-steel design philosophy (AISI-S211-07) and the chord studs

selected are 600S162-054 on the first floor and 600S162-033 on the second floor (nomenclature per AISI-S200). The joists are unblocked and utilize a continuously-braced design philosophy (AISI-S210-07), span the short direction of the building, with 1200S250-097 joists on the second floor and 1200S250-054 joists on the roof. The floors are ledger framed (hung) from the walls with a 1200T200-097 ledger, or rim track, capping the joists.

The selected lateral force resisting system uses OSB sheathed shear walls and diaphragms. For this system the response modification coefficient $R = 6.5$, overstrength factor $\Omega_0 = 3$, and deflection amplification factor $C_d = 4$. The Type I shear walls use back-to-back 600S162-054 chord studs, Simpson S/HDU6 hold downs, and 7/16 in. [1.11 cm] OSB fastened 6 in. [15.24 cm] o.c.. Also, shear anchors connect the bottom tracks of shear walls to the foundation, with 12 in. spacing [30.48 cm] o.c.. Length and location of the shear walls is designed to meet the base shear and architectural constraints resulting in the configuration provided in Fig. 1. The diaphragm is modeled as flexible, per ASCE7-10, and 7/16 in. [1.11 cm] OSB 6 in. [12.54 cm] o.c. is utilized to meet the required strength. See Madsen et al. (2011) for details.

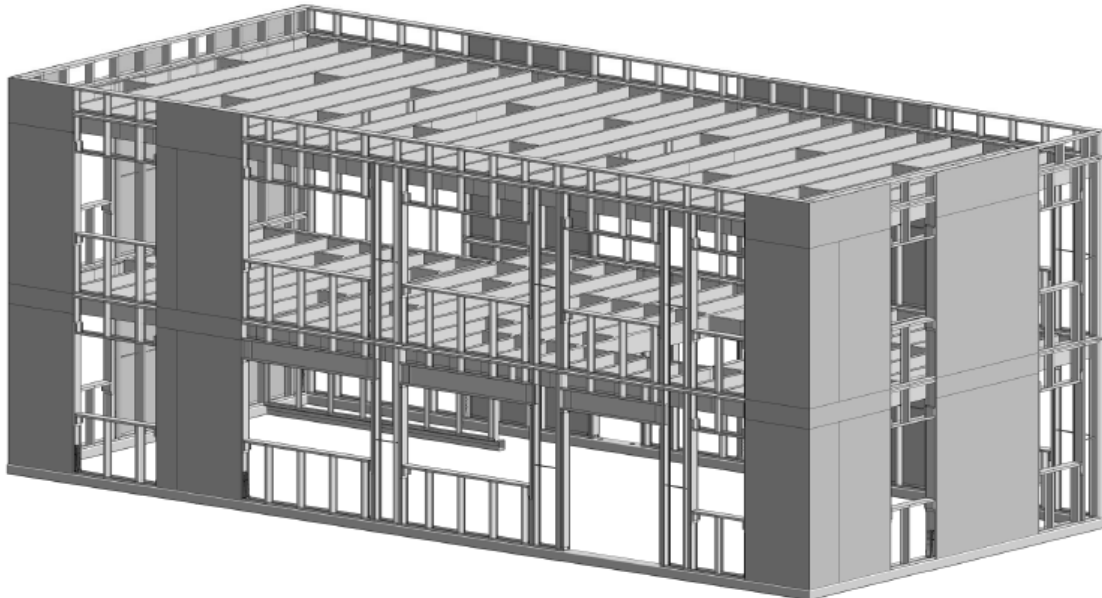


Figure 1: Three-dimensional BIM model of the CFS-NEES building (sheathing shown only for shear walls)

3. Nonlinear OpenSees models of the CFS-NEES building components

This section describes the major components of the structural model constructed for the CFS-NEES building. In comparison with the authors' previous work (Leng et al., 2012), the shear walls are still the major concern; but, additional details are now explicitly modeled and analyzed to provide a better understanding of the full three dimensional building behavior.

3.1 Shear wall models

As an assembly of studs, tracks and sheathing connected by fasteners a shear wall's lateral force resistance mainly comes from the stiffness at the stud-fastener-sheathing connection. Load is transferred from the steel framing to the sheathing through the fasteners. The response of such a system is hysteretic and includes pinching as the fastener tilts and bears into the sheathing causing damage. Tabulated shear wall strengths and an empirical deflection equation that

handles framing, sheathing, and hold down contributions can be found in AISI-S213. Thus, the strength and stiffness (at least up to peak strength) are available in practice.

Simplification of nonlinear shear wall behavior to one or a few degrees of freedom is common: van de Lindt et al. (2004 and 2010), Martínez-Martínez and Xu (2011), Shamim and Rogers (2012), etc. Modeling the shear walls may be carried out by focusing on the relationship between shear force V and lateral deflection Δ , and idealizing the resistance as a single degree of freedom. However, it is desired that the models have a physical width equal to the actual shear wall width in the building and one that causes the chord studs to develop forces similar to the typical truss analogy. A simple way to achieve this goal is to model the shear walls as a pin-connected panel with two diagonals as illustrated in Fig. 2. The boundary members form a mechanism and the lateral stiffness and strength derives directly from the diagonals. In our practice (Leng et al., 2012), the pinned connections are literally realized in 2D models by creating coincident nodes and using multipoint constraints to enforce equal translation but allow for different rotations. In the 3D models, the coincident nodes are ignored for convenience, as linear static analysis shows that the diagonal bracing stiffness greatly exceeds the small moment stiffness of the stud-to-track connection.

Since the shear wall behavior is simplified down to nonlinearity in the diagonal truss elements (Fig. 2) this enables the use of the library of uniaxial hysteretic material models in OpenSees. The one-dimensional stress-strain relationship for the diagonal trusses utilizes the simple stress-strain relation:

$$\sigma = f(\varepsilon) \quad (1)$$

where, after some simple derivation using basic equilibrium and geometry (Leng et al., 2012), the stress and strain can be expressed using the horizontal load V , the axial force in the diagonal F , diagonal cross-sectional area A , and angle θ of the diagonal as

$$\sigma = F / A = V / (2A \cos \theta) \quad (2)$$

and the strain in the diagonal is a function of the horizontal deflection, Δ , and the shear wall width, b , and height, h :

$$\varepsilon = d / l = \Delta \cos \theta / \sqrt{b^2 + h^2} \quad (3)$$

Two forms of the 1D stress-strain relationship, elastic-perfectly-plastic (EPP) and Pinching4 were compared in Leng et al. (2012). EPP, though much simpler with only one linear stiffness and a clear plateau after yielding, has several drawbacks. The major one is the overestimation of energy dissipation under cyclic loading because of its inherent incapability of modeling pinching behavior in the unloading and reloading stages. On the other hand, the Pinching4 model (Lowes and Altoontash, 2003) allows the user to define four points on the backbone curve and pinching behavior as a function of the unloading and reloading stages. A comparison of energy dissipation at selected loops of cyclic loading between Pinching4, EPP simulation and available shear wall tests of Liu et al. (2012) is provided in Fig. 4.

Parameters for the Pinching4 model were arrived at by matching equivalent energy dissipation against shear wall test results by Liu et al. (2012) conducted specifically for the CFS-NEES building. Fig. 3 schematically depicts four points on the backbone curve and illustrates how pinching is defined. The first three points on the backbone curve are set to $(\delta(0.4V_n), 0.4V_n)$, $(\delta(0.8V_n), 0.8V_n)$, and $(\delta(1.0V_n), 1.0V_n)$ and provide the pre-peak envelope, where V_n is the peak shear force in the wall as detailed in the following paragraph. The last (fourth) point on the backbone curve is selected based on the average of Test 4 and 14 from Liu et al. (2012) and results in $(1.004\delta(1.0V_n), 0.197V_n)$. This represents a sharp drop in the post-peak response. The pinching parameters (reloading and unloading) are also selected based on the average of reported results from Liu et al. (2012) and include: $r_s = 0.5$, $r_v = 0.25$, and $u_v = 0.0$ as shown in Fig. 3. (The $V-\Delta$ curve is converted into material properties for the diagonals in Fig. 2 as described in the previous section.)

In this work the shear wall capacity V_n , is based on the testing of Liu et al. (2012), as opposed to the codified values of AISI-S213. From Liu et al. (2012) test 4 and 14 were selected. The test 4 shear wall dimensions are 1.22 m x 2.74 m [4 ft x 9 ft] and Test 14, 2.44 x 2.74 m [8 ft x 9 ft], both with horizontal panel seams at 8' up and OSB sheathing on one side only. The average shear capacity of the wall is $v_n=1013$ plf [14594 N/m] and this is used uniformly for other shear walls, i.e., $V_n = v_n b$. The capacity from test is 23% larger than 825 plf with aspect ratio adjustment from AISI-S213 that was previously used by the authors (Leng et al. 2012).

Another improvement from previous efforts is the explicit modeling of the hold down. The hold down ties the chord stud to the foundation (Fig. 5a). The overturning moment induced by lateral forces in the shear wall are balanced by axial forces in the hold down. Since the hold down is modeled explicitly, the shear wall lateral deflection induced by hold down extension (Δ_h) must be subtracted from total measured horizontal deflection (Δ_t) of the shear wall. The axial force in the hold down due to the overturning moment from lateral force V is Vh/b . The axial displacement of the hold down Δ_h at this force level is computed using the non-linear material model for the hold down (as detailed in next section). The induced lateral displacement is then calculated using geometric relationship as $\Delta_h = d_h/\tan\theta = hd_h/b$. Thus the deflection Δ used in Eqn. 3 is $\Delta = \Delta_t - \Delta_h$. For shear walls with 4 ft [1.22 m] and 8 ft [2.44 m] width, this is done directly since V and Δ are available from test, and Δ_h is available from d_h after V is given. For other shear walls, Δ at the force level V is unknown. The calculation of Δ_h is carried out by interpolation of Δ_h of 4 ft [1.22 m] and 8 ft [2.44 m] wide walls to other widths.

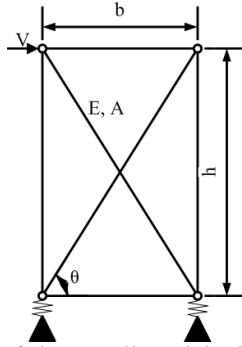


Figure 2: Illustration of shear wall model with separate hold down

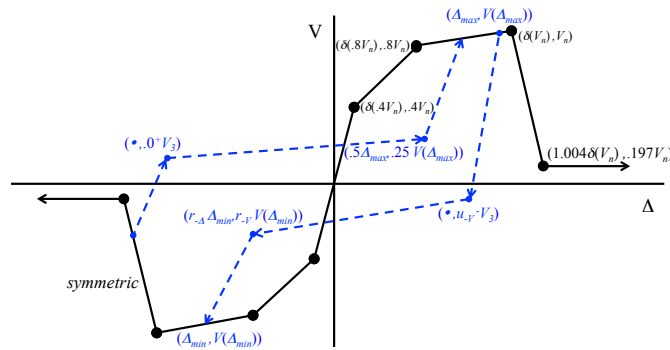


Figure 3: Nonlinear Pinching4 models for shear wall (Leng et al., 2012)

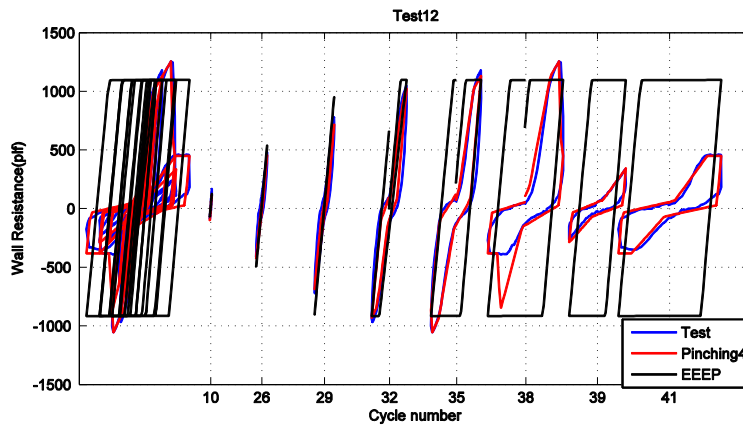


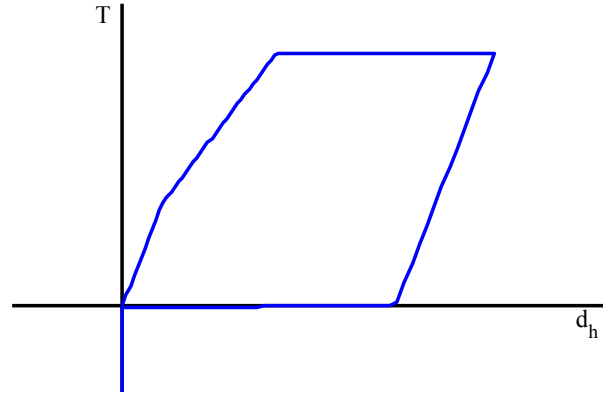
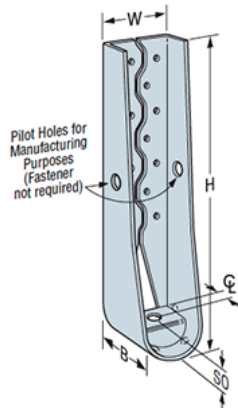
Figure 4: Pinching4 and EEEP model compared with Test 12 of Liu et al. (2012)

3.2 Hold down and shear anchor models

The Simpson S/HDU6 hold down is specified for the CFS-NEES building and was also utilized in the shear wall tests of Liu et al. (2012). Tension tests of the hold down itself are available with stiffness at ASD and LRFD force levels as well as ultimate capacity (Simpson, 2013). These values are used to determine the tension stiffness of the hold down as provided in Table 1. At ultimate the hold down is assumed plastic. (Due to the application of Ω_0 force levels in design the shear panel itself will fail well before the hold down). In compression the hold down is in bearing and an infinite (numerically high) axial stiffness is employed. A Pinching4 model of the hold down is thus created as shown in the load displacement curve of Fig. 5b.

Table 1: Force-displacement relationship of the hold down in tension

Tension Load (lbf)	Deflection (in)	Stiffness (lbf/in)
6125	0.108	56712.96
9785	0.234	29047.62
15005		



(a) Hold down (Simpson Strong-Tie Company Inc., 2013) (b) Axial load-displacement pinching4 model
Figure 5: Hold down and its pinching4 nonlinear material model of axial response

In addition to the hold downs, shear anchors connect the bottom track to the foundation (every 12 in. [30.48 cm] o.c.). In the current model, these anchors are modeled as pin supports. These supports have a high shear stiffness since they engage the axial stiffness of the bottom track. Thus, they are effective in removing shear. However, these shear anchors have a low uplift stiffness (even when fully pinned) since they engage the weak-axis bending of the bottom track. Further, in the current models only the shear walls are modeled, not the gravity walls, so these pin supports only exist at the shear wall locations. When the gravity walls are incorporated into the model these assumptions will need to be revisited.

3.3 Diaphragm models

Diaphragm modeling is an important and influential issue in 3D modeling of the building. A rigid diaphragm and flexible diaphragm represent the two limiting cases: assuming full interaction or no interaction between the shear walls of facing elevations. Initial shear wall design was completed assuming a flexible diaphragm assumption according to ASCE 7 (ASCE, 2005 and 2010) but as detailed in Madsen et al. (2011) the shear walls were also checked for rigid diaphragm conditions and found to be adequate. Since a rigid diaphragm can introduce a strong torsion effect about the vertical axis into the model this condition has been the focus of the 3D modeling to date. (As shown in Fig. 1 the shear walls are not symmetric in location or strength about the perimeter of the building). Further exploration of semi-rigid diaphragm models is needed, and the forthcoming full scale testing is expected to shed additional light on this detail.

3.4 Leaning column models

An important aspect of the 3D modeling is the incorporation of leaning (gravity) columns. As a related outcome, P- Δ effects are considered in the analysis by using co-rotational truss elements as diagonals of the shear walls and co-rotational transformation for other elements. Adding

leaning columns in 3D is more difficult than 2D since the coupling between horizontal bending in two directions and torsion about the vertical axis must be addressed. The approach taken here is to create coincident nodes at the four corners and connect columns with large stiffness to these coincident nodes. These large stiffness leaning columns are forced to behave like a mechanism since their translational degrees of freedom are rigidly tied to the coincident nodes at the corners of the frame while rotations are left free. The mass and gravity of the building is equally distributed to the four corners and are applied at the leaning column ends. Fig. 6 shows the 3D model with details of the usage of coincident node at the southeast corner where two shear walls and leaning columns meet. The addition of leaning columns and P- Δ analysis can yield a more severe but realistic result (Geschwindner, 2002).

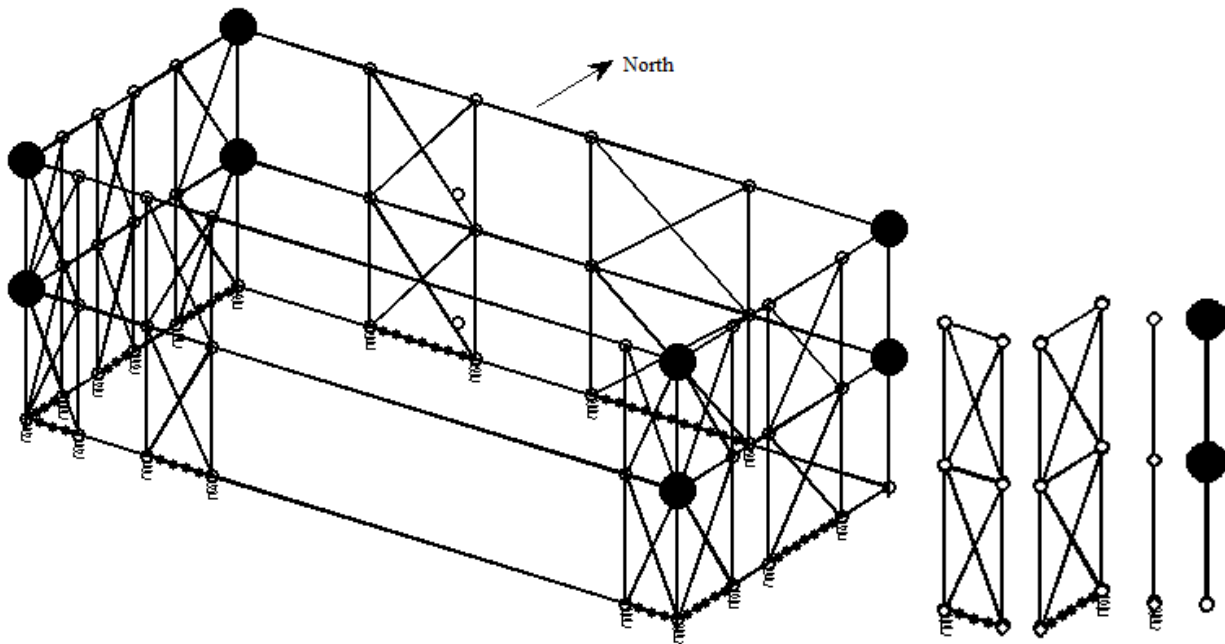


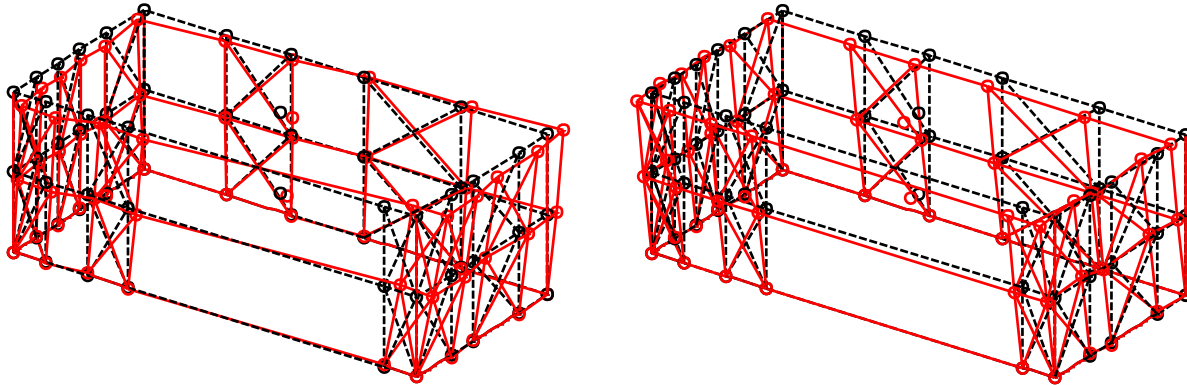
Figure 6: 3D rigid diaphragm state-of-the-art model with an exploded view of the southeast corner

4. Simulation results

Before nonlinear time history analysis and IDA free vibration and pushover analysis is performed to obtain basic understanding of the model behavior. The first three natural periods of the building model are provided in Table 2. All modes include translation in x (West-East), y (North-South), and torsion about z (vertical). Due to the choice of a rigid diaphragm and the asymmetry inherent in the shear wall location and lengths, coupling between bending and torsion can be found in modes shapes of Fig. 7. The use of the shear wall properties based on testing instead of AISI-S213 results in an increased initial stiffness compared with the author's previous model (Leng, et al, 2012). As a result, the first natural period T_1 increase from 0.882 sec. to 0.643 sec. Still, the difference with respect to $T_1 = 0.175$ sec. estimated from ASCE 7 is obvious, and a partial reason for that is that the mass is the gross value (same in both predictions) but the stiffness in the model does not include gravity walls and nonstructural components.

Table 2: Free vibration analysis results of the 3D building model

Mode No.	Natural period (sec.)
1	0.643
2	0.598
3	0.522
4	0.191
5	0.175
6	0.145



(a) Mode 1, $T_1 = 0.643$ sec.

(b) Mode 2, $T_2 = 0.598$ sec.

Figure 7: First and second mode shape of 3D building model

Results of a displacement controlled pushover analysis are provided in Fig. 8. The response presents a reference for the nonlinear behavior of the model from a static analysis. The horizontal displacement in the x direction of the first floor center is controlled, and the base shear is simply the sum of the base shear at the supports of the North and South elevations due to the lack of out of plane stiffness for the shear walls in the West and East elevations. The peak shear force is 32.87 kips [146.21 kN] which equals the sum of the shear wall capacity of the North and South elevations. Peak shear force corresponds with 1.6 in. [4.06 cm] displacement or 1.5% story drift, which is similar to the test results of the shear walls alone. After peak, the sharp drop of base shear indicates failure according to the Pinching4 model response curve.

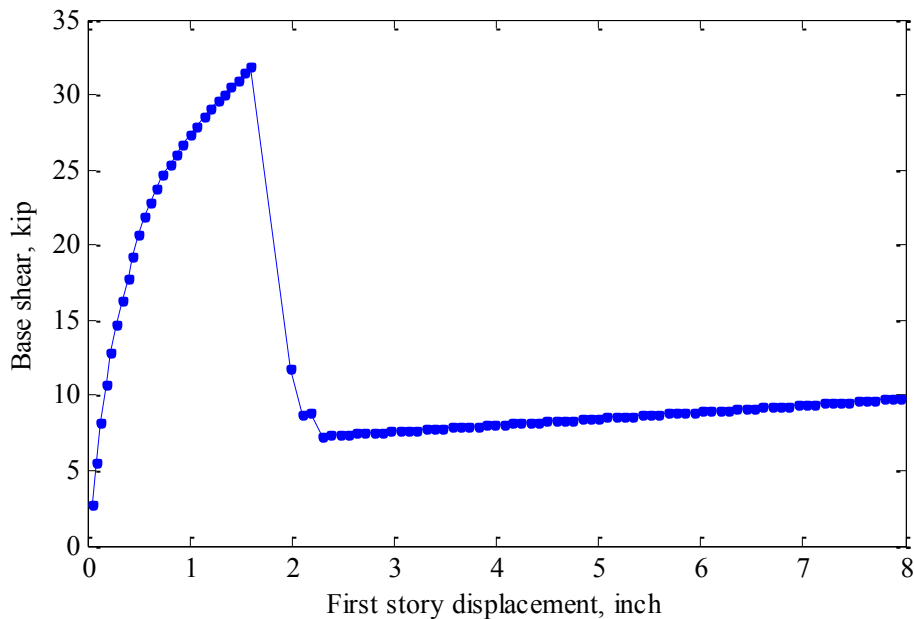


Figure 8: Pushover curve of 3D building model

The simulation results now turn to the IDA procedure. The earthquake excitation suite used in IDA is the FEMA P695 far-field ground motion suite, which is composed of 22 earthquakes recorded around the world. Two horizontal signals in orthogonal directions are provided. In analysis, the excitation is loaded in the x and y directions of the building and then repeated with x and y switched for a total of 44 combinations. Normalization factors from FEMA P695 are applied. The normalized records are scaled up to 8 times the original record to ensure the deformation is large enough to trigger failure in the building. The key recorded response is drift in the two stories. First mode spectral acceleration is the selected intensity measure for the excitation. As discussed by Baker and Cornell (2006), for consistency with conventions in seismology, the S_a of the two axis excitation is defined as the geometrical average of the two S_a under excitation in x and y direction separately. Note, the S_a value does not change when the two earthquakes switch directions.

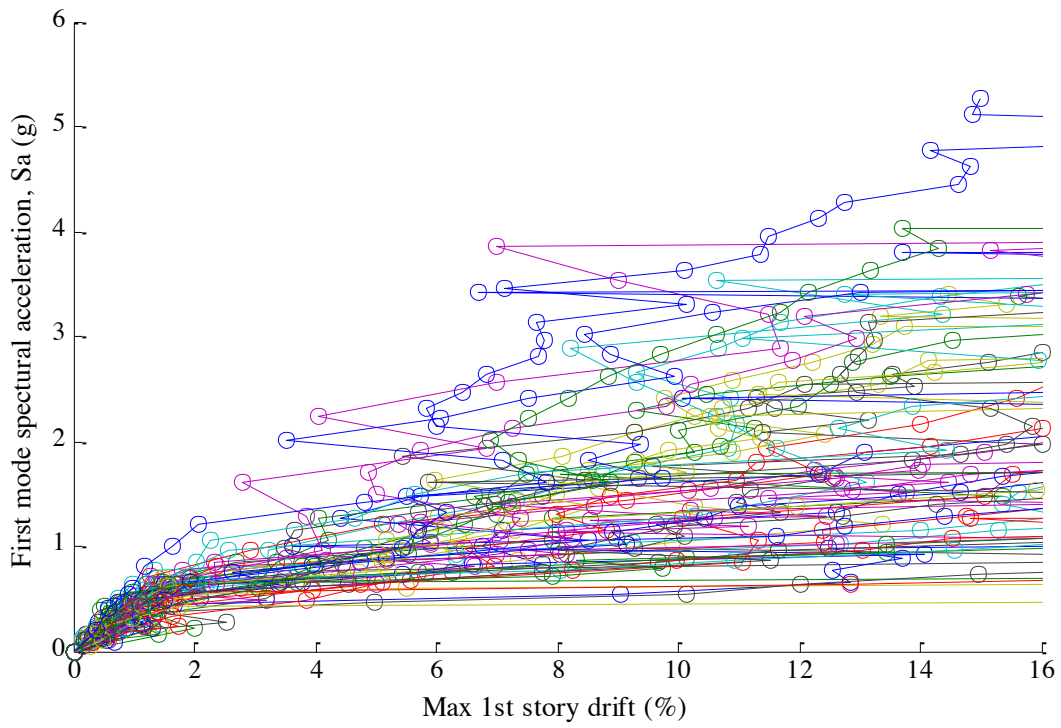
Fig. 9 provides the IDA curves of story drift versus S_a . Dynamic instability does appear at a certain drift (S_a) level. Numerically speaking, dynamic instability implies that the drift becomes unbounded in the simulation, as shown by flat horizontal lines that extend (to infinity) in Fig. 9. The behavior of the two stories is different. For the second story, Fig. 9b, the drift is less than 1.5% of the story drift, while the number is at or about 4% for the first story.

To study this difference, nonlinear time history analyses using different scale levels of the Northridge earthquake recorded at Canoga Park (NGA No. 953) are performed, and the time history of first story drift, base shear, and the deformed shape of building at $t = 2.0$ sec and 5.18 sec (all recorded in the x direction) when the scale factor is 2.0 are provided in Figure 11. The record is chosen because S_a of that excitation is 0.88g, close to elastic design spectrum acceleration of 0.93g. The shear wall diagonals that reach their peak capacities are considered failed and thus marked by (red) dash lines in Fig. 11c and d. The response curve shows that highly nonlinear behavior exists at this scale level. The deformed shape in Fig. 11c and d

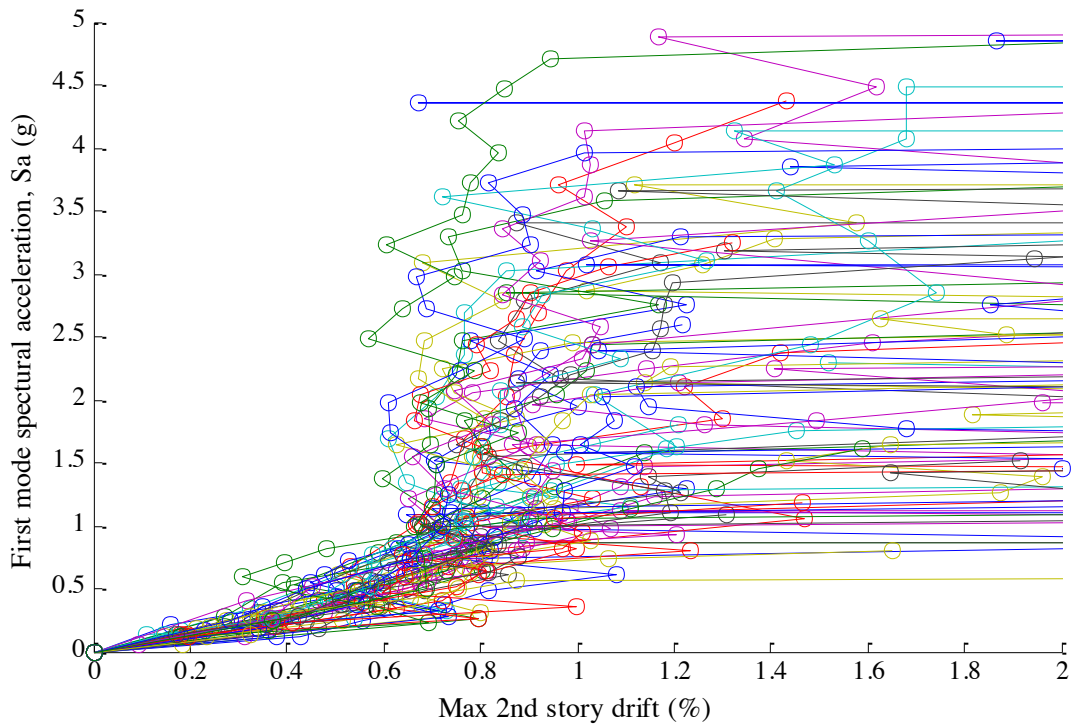
demonstrate that failure of the shear walls is predicted initially in the first story, first at the relatively weaker South elevation, then the North elevation. As the first story fails, the second story shear walls behave like a structure on soft foundations, and thus the story drift of the second story is much smaller compared with the first story. Across the records, failure typically initiates at the first story and thus the assumption made here is to focus on the first story drift for examining stiffness degradation and failure.

Typically a drift limit is provided for collapse prevention. For example light framed wood structures commonly use 7% (Christovasilis et al., 2009) and special steel moment frames may use drifts as high as 9-10% (Applied Technology Council, 2009). Based on the current Pinching4 model and the pushover analysis, the building begins to dramatically lose capacity around 2% drift. This is qualitatively similar to the isolated shear wall testing (Liu et al. 2012), which generally showed drift at peak capacity around 2%, and peak recorded drifts near 4%. Thus, 2% and 4% drift are initial candidates for the failure criterion. Considering the IDA results drifts of most earthquakes appear to be unbounded (unstable) when the first story drift is larger than 4%. If analysts are less conservative and choose to approximately include the stiffness of other components missing in current model, it is possible to imagine drift limits as high as 6 or 8%, comparable to those used in wood structures. Further efforts are needed in drift limit selection.

An alternative failure criterion to drift is the slope of the IDA curve (Vamvatsikos and Cornell, 2004). However, in our current analysis, even when the scale factor is small (usually less than 0.5) and before the nonlinear behavior of the shear wall emerges, isolated IDA curves show fairly large drift and this makes the initial slope of the IDA curves small, leading to artificially high failure predictions. Further investigation reveals that this happens due to numerical sensitivity in the hold down modeling. More refinement in the hold down model and the use of even smaller time steps in the time history analysis (Vamvatsikos and Cornell, 2004) is anticipated to provide better results for future analysis.

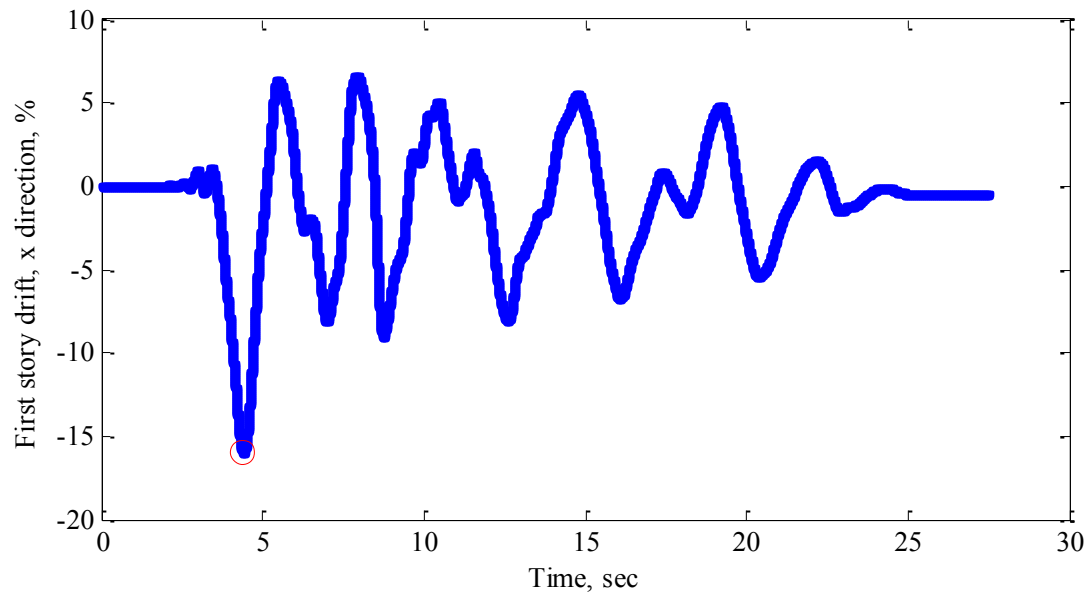


(a) First story

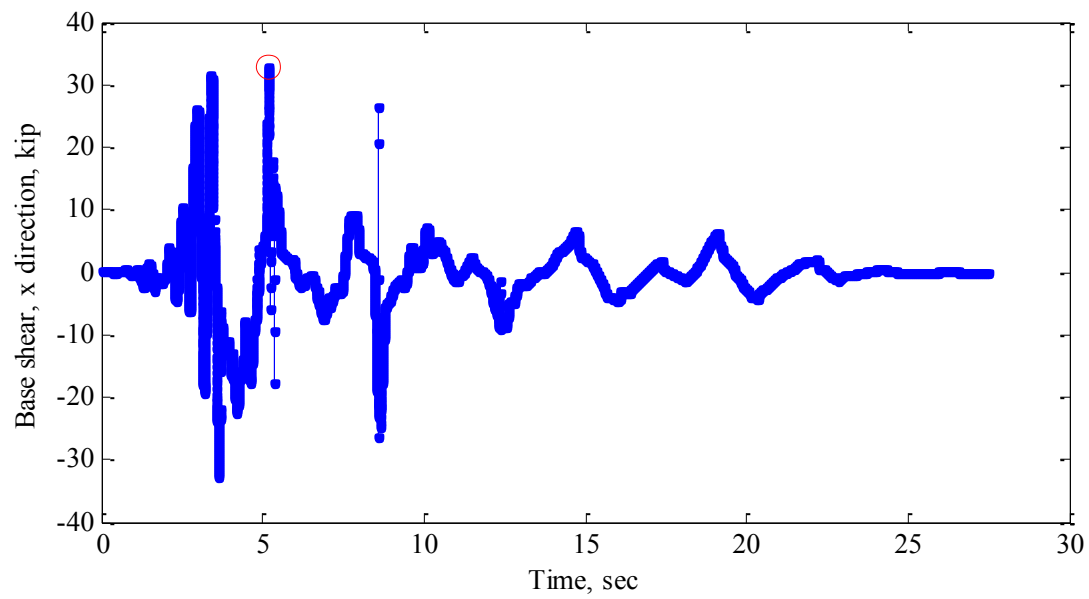


(b) Second story

Figure 9: IDA curves of 3D rigid diaphragm state-of-the-art model 1

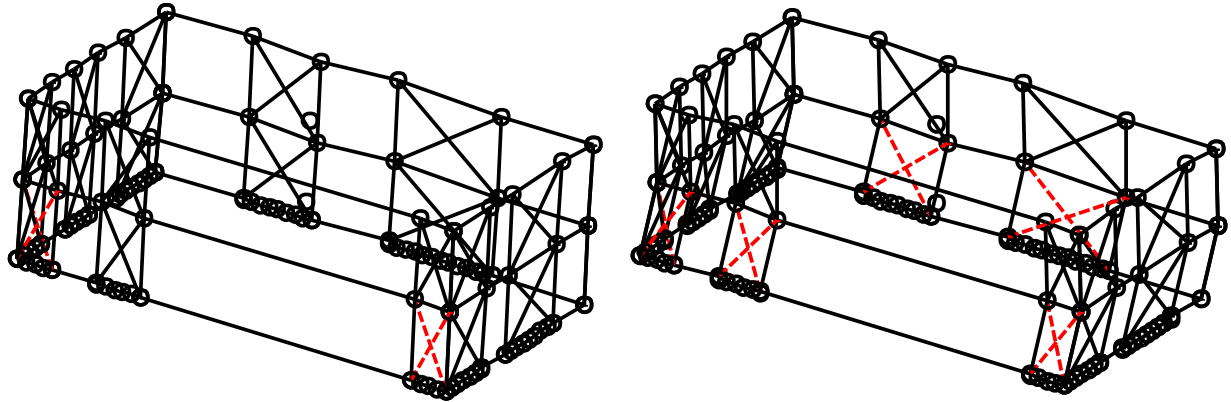


(a) First story drift



(b) Base shear

Figure 10: Time history response curve of the building model under Canoga Park excitation



(a) $t = 2.0$ sec. (b) $t = 5.18$ sec. (max base shear in x direction)
 Figure 11: Deformed shape of the building (displacement magnified 20 times)

Fragility curves based on the various drift limits are presented in Fig. 10. The median collapse capacity (i.e., the S_a level that makes probability of failure equal to 0.5.) is highly sensitive to the selected drift limit. A well-grounded drift limit is key for collapse capacity calculation and design evaluation afterwards. Following the FEMA P695 procedure the median collapse capacity may be used to estimate the seismic response modification factor, R .

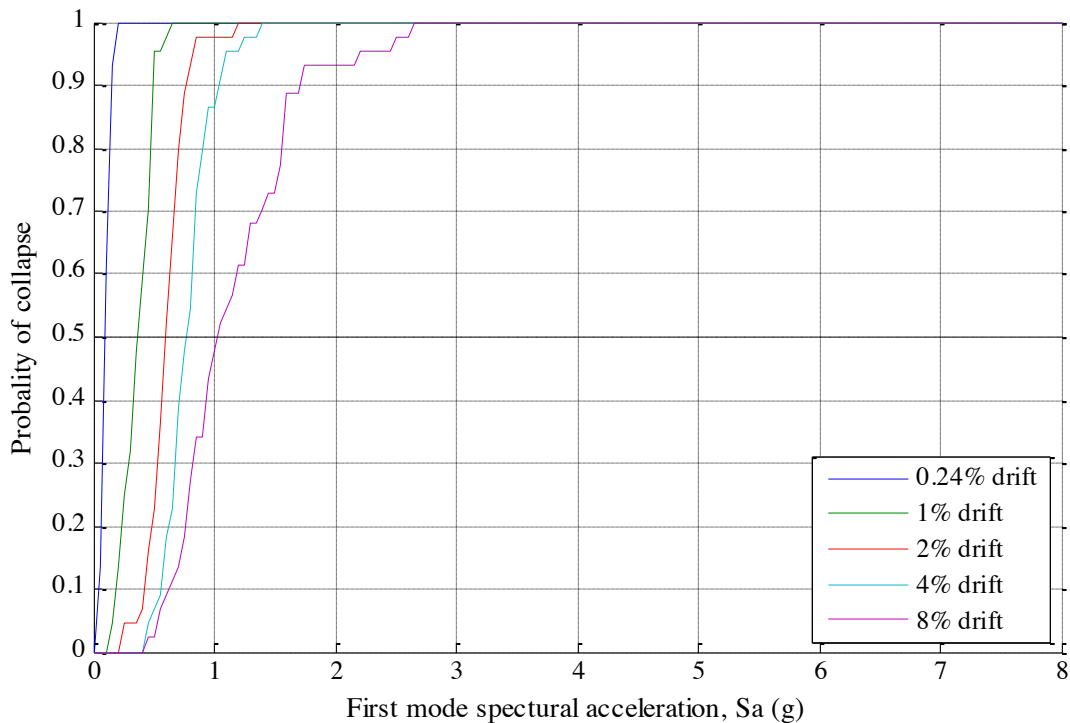


Figure 12: Fragility curve with various drift limits of the first story

To more directly explore the seismic response modification factor, particularly the portion attributed to ductility R_d . The ratio of the elastic to inelastic peak base shear is calculated for every model. Following the previous discussion, a 4% story drift criterion is selected as an approximation of the collapse drift. Then, the ratio of the linear elastic peak base shear over the

nonlinear (Pinching4) peak base shear is computed for each of the 44 excitations. The normalized histogram of the peak base shear ratio, i.e. R_d , is given in Fig. 13. The mean value of the ratio is 4.3. That is the mean expected base shear is about $\frac{1}{4}$ the elastic base shear. For reference the seismic response modification factor $R = 6.5$ (R includes overstrength and other factors that make it by definition larger than the R_d considered here). The dispersion of the calculated R_d ranges from slightly larger than 1 to 10, showing that the record to record difference is significant, which entail analysis using multiple earthquake records and usage of statistical methods in data processing.

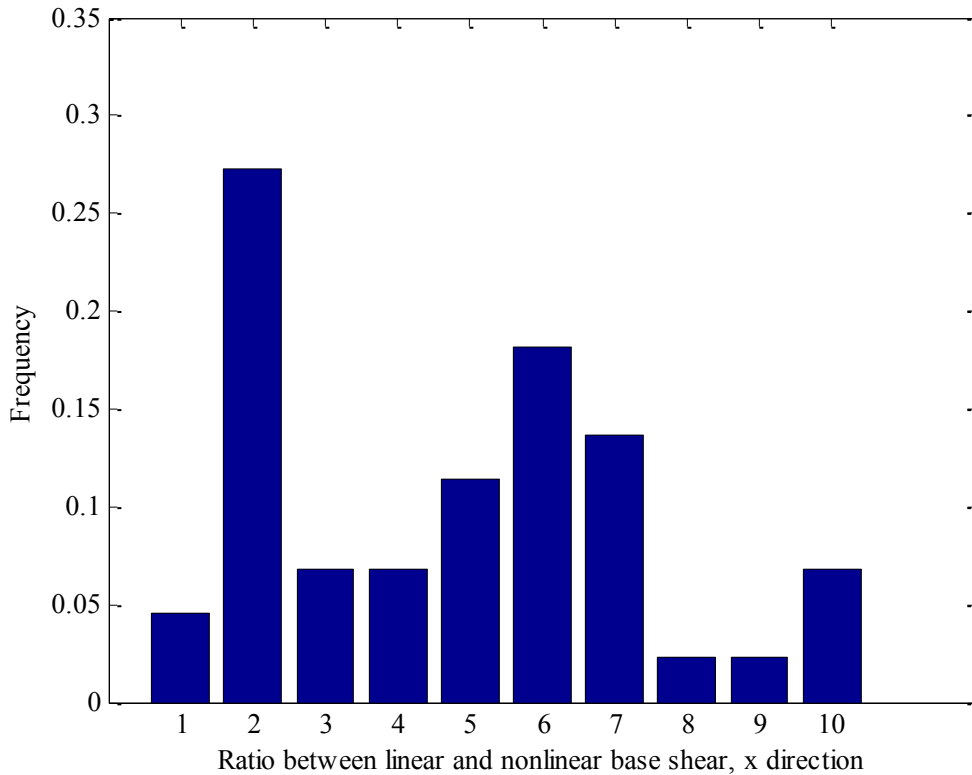


Figure 12: Normalized histogram of linear vs. nonlinear base shear ratio, 4% drift limit

5. Discussion

The results presented above provide insight into the nonlinear response of the CFS-NEES building under earthquake excitation both qualitatively and quantitatively. However, significant work remains both from the modeling perspective and data interpretation. The current model is able to capture the behavior of the shear walls, but more components should be included.

Important components to be included in additional modeling are semi-rigid diaphragms, gravity wall systems, and non-structural components including both interior gypsum sheathing on structural walls, and non-structural walls and finishes. With these effects well simulated, the model will be able to provide a more comprehensive prediction of each structural component and their contribution to the overall behavior of the system. These predictions will be important in understanding forthcoming full-scale testing and exploring the full behavior of CFS framed buildings.

A key consideration for the improved models, and one to be developed in parallel with forthcoming testing is to investigate means to determine the collapse drift limit. In addition, as the model fidelity is increased an important consideration that remains is the determination of the quality of the mode predictions versus the fidelity of the model. Specifically, for designers we seek the simplest possible model that still provides accurate predictions.

6. Conclusion

A nonlinear 3D model in OpenSees of the CFS-NEES building is developed. The building is able to accurately represent the nonlinear behavior of cold-formed steel framed, OSB sheathed, shear wall systems under earthquake excitations. IDA analysis using FEMA P695 ground motion suites shows that the drift limit for collapse prevention can be developed. In the analysis conducted, the average ratio of predicted peak base shear to elastic base shear is approximately 4. Preliminary understanding of the failure mode, which is concentrated in the first story, is presented by probing into the time history of shear wall damage. Improvements to the building model are still possible and needed. Full scale shake table testing of the CFS-NEES building is forthcoming. The model will be used to better understand the testing, and additional calibration of the model based on the test results is also expected.

Acknowledgments

The authors are grateful to George E. Brown, Jr. Network for Earthquake Engineering Simulation (NEES) for the sponsorship. Thanks are extended to Rob Madsen at Devco Engineering for his design work of the archetype building. This paper was prepared as part of the U.S. National Science Foundation sponsored CFS-NEES project: NSF-CMMI-1041578: NEESR-CR: Enabling Performance-Based Seismic Design of Multi-Story Cold-Formed Steel Structures. The project also received supplementary support and funding from the American Iron and Steel Institute. Project updates are available at www.ce.jhu.edu/cfsnees. Any opinions, findings, and conclusions or recommendations expressed in this publication are those of the author(s) and do not necessarily reflect the views of the National Science Foundation, nor the American Iron and Steel Institute.

References

- American Iron and Steel Institute. "North American standard for cold-formed steel framing - wall stud design, 2007 edition (AISI S211-07 ed.)." Washington, DC: American Iron and Steel Institute.
- American Iron and Steel Institute. (2007). "North American specification for the design of cold-formed steel structural members, 2007 edition with supplement 2 (AISI S100-07 w/S2-10 ed.)." Washington, DC: American Iron and Steel Institute.
- American Iron and Steel Institute. (2007). "North American standard for cold-formed steel framing - floor and roof system design, 2007 edition (AISI S210-07 ed.)." Washington, DC: American Iron and Steel Institute.
- American Iron and Steel Institute. (2007). "North American standard for cold-formed steel framing - general provisions, 2007 edition (AISI S200-07 ed.)." Washington, DC: American Iron and Steel Institute.
- American Iron and Steel Institute. (2009). "North American standard for cold-formed steel framing - lateral design 2007 edition with supplement no. 1 and commentary (AISI S213-07-SI-09 ed.)." Washington, DC: American Iron and Steel Institute.
- American Society of Civil Engineers (ASCE). (2005). "Minimum design loads for buildings and other structures (ASCE/SEI 7-05 ed.)." Reston, VA: American Society of Civil Engineers.

- American Society of Civil Engineers (ASCE). (2007). "Seismic rehabilitation of existing buildings (ASCE/SEI 41-06 ed.)." Reston, VA: American Society of Civil Engineers.
- American Society of Civil Engineers (ASCE). (2010). "Minimum design loads for buildings and other structures (ASCE/SEI 7-10 ed.)." Reston, VA: American Society of Civil Engineers.
- Applied Technology Council. (2009). "Quantification of building seismic performance factors." No. FEMA P695
- Baker, J. W., & Cornell, C. A. (2006). "Which spectral acceleration are you using?" *Earthquake Spectra*, 22(2), 293-312.
- Christovasilis, I. P., Filiatrault, A., Constantinou, M. C., & Wanitkorkul, A. (2009). "Incremental dynamic analysis of woodframe buildings." *Earthquake Engineering & Structural Dynamics*, 38(4), 477-496.
- Geschwindner, L. F. (2002). "A practical look at frame analysis, stability and leaning columns." *Engineering Journal*, 39(4), 167-181.
- Leng, J., Schafer, B. W., & Buonopane, S. G. (2012). "Seismic computational analysis of CFS-NEES building." *Proceedings of 21th International Specialty Conference on Cold-Formed Steel Structures - Recent Research and Developments in Cold-Formed Steel Design and Construction*, St. Louis, MO. pp. 801-820.
- Liu, P., Peterman, K. D., Yu, C., & Schafer, B. W. (2012). "Characterization of cold-formed steel shear wall behavior under cyclic loading for the CFS-NEES building." *Proceedings of 21th International Specialty Conference on Cold-Formed Steel Structures - Recent Research and Developments in Cold-Formed Steel Design and Construction*, St. Louis, MO. pp. 703-722.
- Lowes, L. N., & Altoontash, A. (2003). "Modeling reinforced-concrete beam-column joints subjected to cyclic loading." *Journal of Structural Engineering*, 129(12), 1686-1697.
- Madsen, R. L., Nakata, N., & Schafer, B. W. (2011). "CFS-NEES building structural design narrative." No. CFS-NEES-RR01)
- Martínez-Martínez, J., & Xu, L. (2011). "Simplified nonlinear finite element analysis of buildings with CFS shear wall panels." *Journal of Constructional Steel Research*, 67(4), 565-575.
- McKenna, F. et al. (2011). "Open system for earthquake engineering simulation (OpenSees) (2.3.2 ed.)." Berkeley, CA: Pacific Earthquake Engineering Research Center, University of California.
- Peng, J., Chan, S., & Wu, C. (2007). "Effects of geometrical shape and incremental loads on scaffold systems." *Journal of Constructional Steel Research*, 63(4), 448-459.
- Shamim, I., & Rogers, C. A. (2012). "Numerical modelling and calibration of CFS framed shear walls under dynamic loading." *Proceedings of 21th International Specialty Conference on Cold-Formed Steel Structures - Recent Research and Developments in Cold-Formed Steel Design and Construction*, St. Louis, MO. pp. 687-701.
- Simpson Strong-Tie Company Inc. (2013). "Load table of S/HDU hold downs." Simpson Strong-Tie Company Inc. http://www.strongtie.com/products/cfs/s_hdu.asp
- Vamvatsikos, D., & Cornell, C. A. (2002). "Incremental dynamic analysis." *Earthquake Engineering & Structural Dynamics*, 31(3), 491-514.
- Vamvatsikos, D., & Cornell, C. A. (2004). "Applied incremental dynamic analysis." *Earthquake Spectra*, 20(2), 523-553.
- van de Lindt, J. W. (2004). Evolution of wood shear wall testing, modeling, and reliability analysis: Bibliography. *Practice Periodical on Structural Design and Construction*, 9(1), 44-53.
- van de Lindt, J. W., Pei, S., Liu, H., & Filiatrault, A. (2010). Three-dimensional seismic response of a full-scale light-frame wood building: Numerical study. *Journal of Structural Engineering*, 136(1), 56-65.